

# Lawrence Berkeley National Laboratory

## Recent Work

### Title

Rich Chemistry in Inorganic Halide Perovskite Nanostructures.

### Permalink

<https://escholarship.org/uc/item/7ns2c045>

### Journal

Advanced materials (Deerfield Beach, Fla.), 30(48)

### ISSN

0935-9648

### Authors

Huang, Jianmei  
Lai, Minliang  
Lin, Jia  
et al.

### Publication Date

2018-11-01

### DOI

10.1002/adma.201802856

Peer reviewed

# Rich Chemistry in Inorganic Halide Perovskite Nanostructures

Jianmei Huang, Minliang Lai, Jia Lin, and Peidong Yang\*

Halide perovskites have emerged as a class of promising semiconductor materials owing to their remarkable optoelectronic properties exhibiting in solar cells, light-emitting diodes, semiconductor lasers, etc. Inorganic halide perovskites are attracting increasing attention because of the higher stability toward moisture, light, and heat as compared with their organic–inorganic hybrid counterparts. In particular, inorganic halide perovskite nanomaterials provide controllable morphology, tunable optoelectronic properties, and improved quantum efficiency. Here, the development controlled synthesis of desired inorganic halide perovskite nanostructures by various chemical approaches is described. Utilizing these nanostructures as platforms, anion exchange chemistry for wide compositional and optical tunabilities is described, and the rich structural phase transition phenomenon and mechanism investigated systematically. Furthermore, these nanostructures and extracted knowledge are applied to design photonic, photovoltaic, and thermoelectric devices. Finally, future directions and challenges toward improvement of the optical, electrical, and optoelectronic properties, exploration of the anion and cation exchange kinetics, and alleviation of the stability and toxicity issues in inorganic lead based halide perovskites are discussed to provide an outlook on this promising field.

## 1. Introduction

Halide perovskites, with a typical structure of  $ABX_3$  ( $A = CH_3NH_3^+$ ,  $CH(NH_2)_2^+$ ,  $Cs^+$ ;  $B = Pb^{2+}$ ,  $Sn^{2+}$ ;  $X = Cl^-$ ,  $Br^-$ ,  $I^-$ ), have been demonstrated to be a class of promising

semiconductors as their remarkable structure related optoelectronic properties including long carrier diffusion length, high absorption coefficient, and high photovoltaic and photoluminescence (PL) efficiencies due to the defect tolerant characteristic of this material type.<sup>[1]</sup> Based on these outstanding features and the low-temperature solution processability, halide perovskites have attracted considerable attentions in the past several years. Tremendous efforts have been devoted to making high performance halide perovskite based devices including solar cells,<sup>[2]</sup> light emitting diodes,<sup>[3]</sup> and semiconductor lasers,<sup>[4]</sup> and many breakthroughs have been achieved. Especially, the power conversion efficiency records in solar cells are constantly being refreshed,<sup>[5]</sup> and the highest certified efficiency reaches 22.7% during the time of this article writing.<sup>[6]</sup>

Inorganic halide perovskites consisting of inorganic A site cations such as  $Cs^+$  have been demonstrated with improved stability toward moisture, light, and heat as compared with organic–inorganic hybrid counterparts.<sup>[7]</sup> Therefore, a lot of studies have been focused on the growth of inorganic halide perovskite nanostructures using different strategies including colloidal synthesis, anti-solvent, substrate evaporation, and substrate vapor transport.<sup>[8]</sup> By controlling the rich reaction chemistry in the preparation of inorganic halide perovskites, high quality and well-defined morphologies of zero-dimensional (0D) quantum dots (QDs),<sup>[9]</sup> one-dimensional (1D) nanowires (NWs),<sup>[10]</sup> and two-dimensional (2D) nanoplates (NPLs) or nanosheets (NSs)<sup>[11]</sup> have been achieved. Inorganic halide perovskites in nanosize have shown superior optical, electrical, and optoelectronic properties including enhanced exciton binding energy, strong absorption, and high PL quantum yield (PLQY),<sup>[8]</sup> which offer excellent platforms for distinct fundamental research and further development for future applications.


Here, we summarize our recent research progress from Prof. Peidong Yang's group mainly on the topic of inorganic halide perovskite nanostructures (Figure 1). We develop controlled synthesis of desired nanostructures (0D QDs, 1D NWs, and 2D NPLs) by various chemical approaches. The anion exchange chemistry was demonstrated in these nanostructures. We further study the rich structural phase transition phenomenon and disclose their mechanisms. Moreover, we apply these nanostructures and fundamental understanding

Dr. J. Huang, M. Lai, Dr. J. Lin, Prof. P. Yang  
Department of Chemistry  
University of California  
Berkeley, CA 94720, USA  
E-mail: p\_yang@berkeley.edu

Prof. P. Yang  
Materials Sciences Division  
Lawrence Berkeley National Laboratory  
Berkeley, CA 94720, USA

Prof. P. Yang  
Kavli Energy NanoScience Institute  
Berkeley, CA 94720, USA

Prof. P. Yang  
Department of Materials Science and Engineering  
University of California  
Berkeley, CA 94720, USA

 The ORCID identification number(s) for the author(s) of this article can be found under <https://doi.org/10.1002/adma.201802856>.

DOI: 10.1002/adma.201802856

to design photonic, photovoltaic, and thermoelectric devices. Finally, we will discuss the future directions and challenges toward improvement of the optical, electrical and optoelectronic properties, exploration of the anion and the cation exchange kinetics, and alleviation of stability and toxicity issues in lead based halide perovskites, in order to provide an outlook on this emerging field.

## 2. Controlled Synthesis of 1D and 2D Halide Perovskite Nanostructures

It is known that semiconductors at the nanoscale exhibit dimensionality dependent optical, electrical, and optoelectronic properties. For example, the constraint of dimensionality would result in the quantum size effect, which would change the electronic band structures and their behaviors.<sup>[8,12]</sup> In 0D QDs, electrons are quantum confined in three directions; in 1D NWs, electrons are quantum confined in two (perpendicular) directions; while in 2D NPLs or NSs, electrons are quantum confined in one direction. Semiconducting 0D QDs,<sup>[13]</sup> 1D NWs,<sup>[14]</sup> and 2D NPLs or NSs<sup>[15]</sup> have shown the unique optical and electrical properties superior to those corresponding bulk counterparts.

Our group mainly focuses on the fundamental study toward 1D NWs and 2D NPLs or NSs of inorganic halide perovskites. We will introduce here the development of various synthesis strategies toward high quality 1D NWs with well-defined morphology and 2D ultrathin NSs. NWs with different dimensions can be synthesized by both colloidal synthesis and substrate evaporation approaches, while for NSs, a modified substrate method has been proposed, leading to the precise control of the sheet thickness, down to few atomic layers.

### 2.1. Colloidal Synthesis Approach

#### 2.1.1. Growth of CsPbX<sub>3</sub> Nanowires

Semiconducting NWs exhibit many interesting properties beyond those in 3D or bulk materials and have attracted considerable attention as they have potential applications in many fields such as optoelectronics,<sup>[16]</sup> photovoltaics,<sup>[17]</sup> thermoelectrics,<sup>[18]</sup> and sensing.<sup>[19]</sup> In halide perovskites field, it is reported that methylammonium lead halide perovskites NWs, grown via a surface-initiated solution method have exhibited low lasing thresholds and high PL efficiency, and broad optical tunability across the whole visible range.<sup>[4c]</sup> However, the synthesis and fundamental study of the optical properties of uniform inorganic lead halide perovskites NWs, which are expected to own higher stability toward moisture and light and thus more robust for various applications, are lacking.

In the typical lead (Pb) halide cubic perovskite structure, Pb is located in the center of the PbX<sub>6</sub> octahedron, which is connected corner to corner into a 3D network, and A cation occupies the cuboctahedral cavity defined by eight neighboring octahedra. It is thus facile to grow bulk single crystals and nanostructured crystals into a cube shape due to the cubic crystal structure. The promotion of the template-free and catalyst-free anisotropic growth of 1D NWs is of our great interest and an important beginning step.



**Jianmei Huang** received her Ph.D. in materials processing engineering from South China University of Technology under the supervision of Prof. Ouyang Liuzhang and Prof. Min Zhu. During her Ph.D. period, as a visiting student, she studied at Fudan University (2013–2014) under the supervision of Prof. Xuebin

Yu, and ETH Domain (Empa and EPFL, 2014–2015) under the supervision of Prof. Andreas Züttel. Her Ph.D. research focused on developing novel metal borohydrides for hydrogen storage. She currently works as a postdoctoral researcher in Prof. Peidong Yang's group at University of California, Berkeley. Her current research focuses on developing novel inorganic halide perovskite nanomaterials for optoelectronic applications.



**Minliang Lai** received his B.Sc. in materials physics from University of Science and Technology of China (USTC) in 2014. He is currently a Ph.D. candidate in Prof. Peidong Yang's group at University of California at Berkeley. His research focuses on developing, fundamental

study and optoelectronic applications of inorganic halide perovskite nanostructures.



**Peidong Yang** received a B.S. in chemistry from University of Science and Technology of China in 1993 and a Ph.D. in chemistry from Harvard University in 1997. He did postdoctoral research at University of California, Santa Barbara before joining the faculty in the Department of Chemistry at the University of California, Berkeley in 1999.

He is currently professor in the Department of Chemistry, Materials Science and Engineering and a senior faculty scientist at the Lawrence Berkeley National Laboratory. He is S. K. and Angela Chan Distinguished Chair Professor in Energy. He is the director for California Research Alliance by BASF, and co-director for the Kavli Energy Nanoscience Institute.

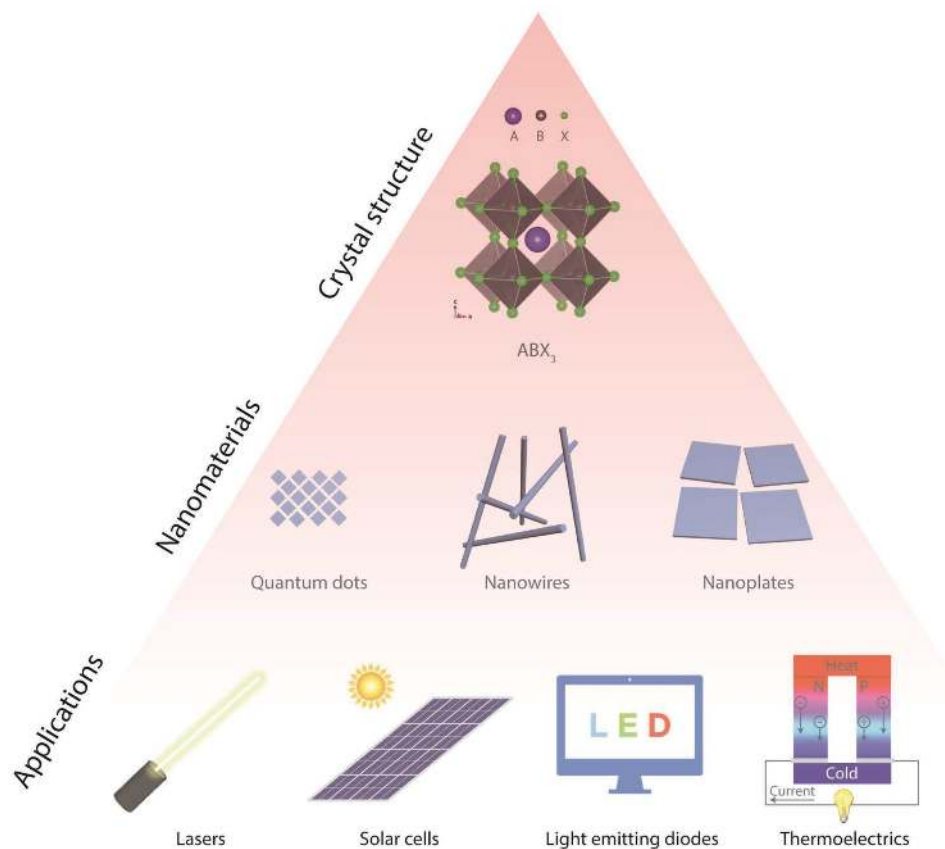


**Figure 1.** Schematics of the design from typical inorganic halide perovskite crystal structure ( $ABX_3$ ) to various nanostructures (0D QDs, 1D NWs, 2D NPLs), and then integration of different applications including lasers, solar cells, light emitting diodes, and thermoelectric devices.

$CsPbX_3$  ( $X = Cl^-$ ,  $Br^-$ , or  $I^-$ ) is a typical inorganic lead halide perovskite material. The colloidal synthesis of  $CsPbX_3$  nanostructures makes full use of the advantages of the ionic bonding nature in these compounds. Kovalenko group has developed a colloidal method to synthesize single crystalline  $CsPbX_3$  0D monodisperse nanocubes (NCs) by controlling the precipitation of  $Cs^+$ ,  $Pb^{2+}$ , and  $X^-$  ions into  $CsPbX_3$  by hot injection of Cs-oleate into a high boiling solvent (octadecene) with  $PbX_2$  in the presence of oleic acid and oleylamine (Figure 2b iii).<sup>[9]</sup> Inspired by this method, our group has recently developed a facile and controllable way for the synthesis of 1D NWs in the absence of hard templates and catalysts.<sup>[10a,11a]</sup>

By extending the reaction duration of NCs synthesis,  $CsPbBr_3$  NWs with a uniform diameter of  $10 \pm 2$  nm and a length up to 5  $\mu m$  were successfully synthesized (Figure 2b i).<sup>[10a]</sup> The morphology evolves from NCs at the initial stage (<10 min) to the mixtures of NCs, NWs, and NSs in the medium stage (10–40 min), and then to the NWs as a dominated product in a later stage (40–60 min). These NWs show single-crystalline nature, grow uniformly along  $\langle 110 \rangle$  direction, and crystallize in the orthorhombic phase. The formation mechanism of NWs is most likely to be a surfactant-directed 1D growth mode after study on the controlling of the reaction temperature, precursor concentration, and ligands concentration and composition. A deeper understanding of the growth mechanism still needs further study. This synthesis method can also be applied to the

growth of  $CsPbCl_3$  and  $CsPbI_3$  NWs. By replacing oleic acid surfactant with octylamine, the yield of  $CsPbBr_3$  NWs can be highly increased and the purity of the product can reach about 90% after simple purification.<sup>[20]</sup>  $CsPbBr_3$  NWs with a diameter of  $\approx 10$  nm show an absorption onset of 521 nm (2.38 eV) and a narrow PL emission spectrum with a moderate quantum confinement (Figure 2a i) (a 60 meV blue-shift compared to the bulk counterparts) because of the small nanowire diameters. These NWs with a well-defined morphology can be a platform for the investigation of electronic and thermoelectronic properties and the development of optoelectronic applications.

### 2.1.2. Growth of Ultrathin Nanowires

Semiconductor NWs with an ultrathin diameter down to the atomic level (2–3 nm) and lengths up to micrometer scale have attracted significant interest because of their high surface area, increased colloidal stability, controlled surface chemistry, and unique physical properties.<sup>[21]</sup> Ultrathin semiconductor NWs with a diameter below their Bohr radius have been demonstrated to show strong quantum size effects, which are of great importance for optoelectronic applications.<sup>[22]</sup> The exciton Bohr radius of  $CsPbBr_3$  is calculated to be 7 nm,<sup>[9]</sup> which is the reason that only a small degree of quantum confinement was observed in the  $CsPbBr_3$  NWs with a diameter

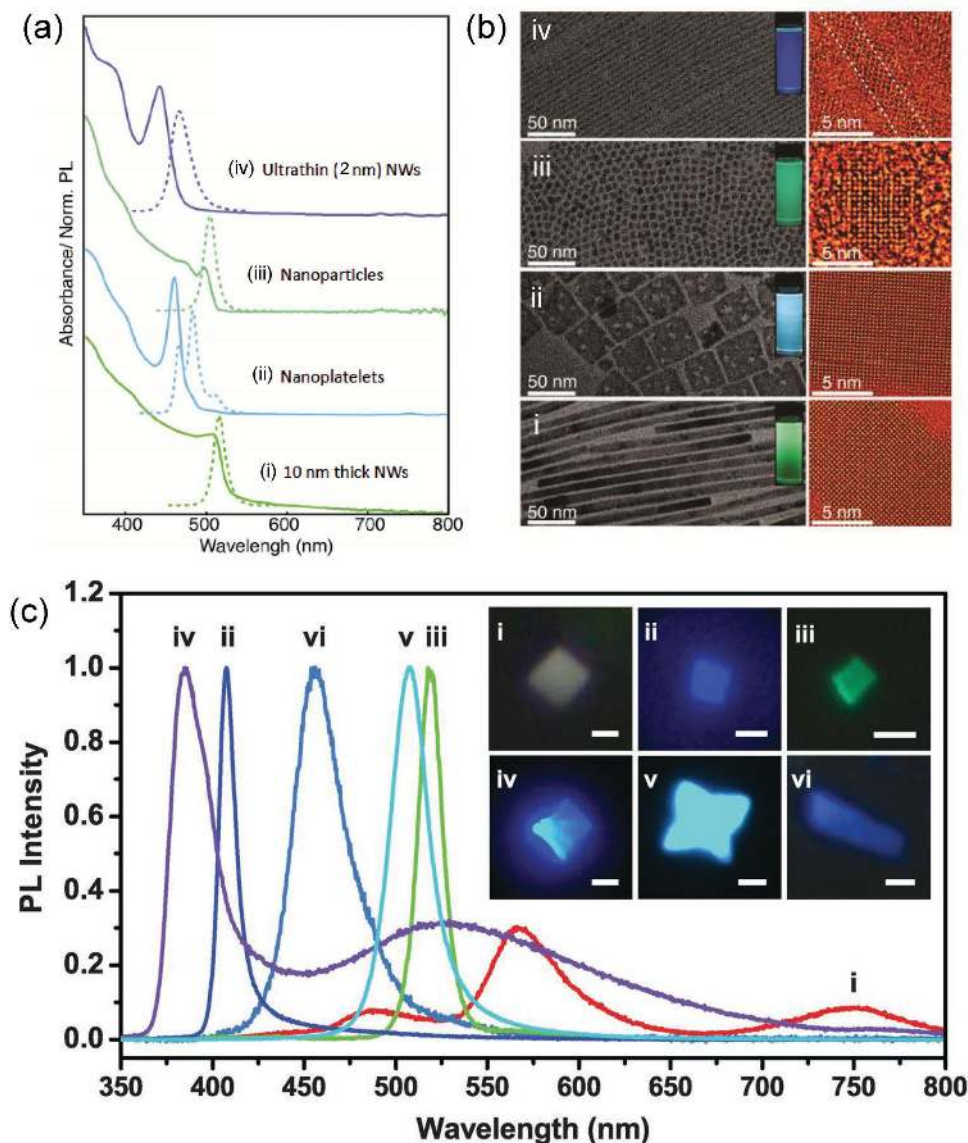


**Figure 2.** a) Optical absorption (solid line), PL (dashed line) spectra, and b) low-resolution TEM and AC-HRTEM images of CsPbBr<sub>3</sub> (i) 10 nm thick NWs, (ii) NPLs, (iii) NCs, and (iv) ultrathin NWs. The insets show the images of the corresponding colloidal solutions under UV illumination ( $\lambda = 365$  nm). Reproduced with permission.<sup>[10b]</sup> Copyright 2016, ACS. c) PL spectra of 2D perovskite sheets with different compositions: (i) (C<sub>4</sub>H<sub>9</sub>NH<sub>3</sub>)<sub>2</sub>PbCl<sub>4</sub>, (ii) (C<sub>4</sub>H<sub>9</sub>NH<sub>3</sub>)<sub>2</sub>PbBr<sub>4</sub>, (iii) (C<sub>4</sub>H<sub>9</sub>NH<sub>3</sub>)<sub>2</sub>PbI<sub>4</sub>, (iv) (C<sub>4</sub>H<sub>9</sub>NH<sub>3</sub>)<sub>2</sub>PbCl<sub>2</sub>Br<sub>2</sub>, (v) (C<sub>4</sub>H<sub>9</sub>NH<sub>3</sub>)<sub>2</sub>PbBr<sub>2</sub>I<sub>2</sub>, and (vi) (C<sub>4</sub>H<sub>9</sub>NH<sub>3</sub>)<sub>2</sub>(CH<sub>3</sub>NH<sub>3</sub>)Pb<sub>2</sub>Br<sub>7</sub>. The corresponding PL images are shown in the inset. Scale bars: 2  $\mu$ m for (i) to (v) and 10  $\mu$ m for (vi). Reproduced with permission.<sup>[29]</sup> Copyright 2015, AAAS.

of  $\approx 10$  nm. To achieve the strong quantum confinement effect in 1D halide perovskite NWs, the diameter should be largely reduced, well below their Bohr radius.

Based on this motivation, we choose CsPbBr<sub>3</sub> NWs as a model system and have successfully synthesized high uniform and single-crystalline ultrathin CsPbBr<sub>3</sub> NWs with a diameter of  $2.2 \pm 0.2$  nm (Figure 2b iv) by modifying the synthesis parameters based on the recipe of  $\approx 10$  nm thick CsPbBr<sub>3</sub> NWs.<sup>[10b]</sup> We found that adding the dodecylamine is important for obtaining the ultrathin nanowires, probably due to the role of ligand in the growth kinetic. For more insight of the growth mechanism of ultrathin nanowires still need further investigation. The UV-vis absorption and PL spectra of the ultrathin NWs revealed a larger blue shift to 442 nm (2.81 eV) and 465 nm (2.67 eV) compared to those of the  $\approx 10$  nm

thick NWs, respectively, indicating the existence of a very strong 2D quantum confinement effect (Figure 2a iv). The larger Stokes shift found in the ultrathin NWs implies that the size-dependent band-edge electronic structure of CsPbBr<sub>3</sub>. The PLQY of ultrathin NWs after purification and surface treatment was measured to be around 30%, lower than the PLQY of the CsPbBr<sub>3</sub> NWs (53%) with a diameter of  $\approx 10$  nm, which is probably because of the increased surface states from the higher surface area.

The PL peak position of ultrathin NWs is located at 465 nm, which is quite similar to the CsPbBr<sub>3</sub> NPLs in thickness of 4-unit-cell (2.33 nm) synthesized by lowering the reaction temperature compared to the synthesis of NCs (Figure 2a ii).<sup>[11a]</sup> We can also visualize the pristine structure of ultrathin CsPbBr<sub>3</sub> NPLs in atomic resolution by applying low dose-rate in-line

holography, which combines aberration-corrected high-resolution transmission electron microscopy (AC-HRTEM) with exit-wave reconstruction.<sup>[23]</sup> This technique we developed minimizes the electron beam-induced sample variation by effectively adjusting electron beam-induced object excitations, and achieves quantitative structure determination using the phase information of the reconstructed exit-wave function. This method opens new routes for atomic resolution imaging of beam sensitive materials.

## 2.2. Substrate-Crystallization Approach

### 2.2.1. Large Sized CsBX<sub>3</sub> Nanowires

The relatively weak ionic bonding in halide perovskites enables direct crystallization of halide perovskites from soluble precursors in polar solvents. We have developed a surfactant-free substrate-guided method to grow single-crystalline inorganic halide perovskite nanostructures.<sup>[24]</sup> A substrate (a piece of glass or coated with poly(3,4-ethylenedioxythiophene) polystyrene sulfonate (PEDOT:PSS) for wetting modification) is spin coated with a thin film of PbX<sub>2</sub>, and then immersed in a dilute CsX solution. Pb precursor slowly dissolves and recrystallizes with surrounding CsX to form CsPbX<sub>3</sub> perovskite NWs. The limited solubility of the Pb precursor in surrounding solution should be the key factor for the growth. Meanwhile, in the case of CsSnX<sub>3</sub>, we apply a reverse sequence that a pre-coated CsX film is immersed into SnX<sub>2</sub> isopropyl alcohol solution because of the higher solubility of Sn precursors.<sup>[25]</sup> These single-crystalline individual large-sized perovskite NWs (with a few hundred nm width and micron scale length) are a good platform to study the phase transition chemistry, optical and transport properties, as well as nanoscale optoelectronic applications, which we will further discuss in the following sessions.

### 2.2.2. Atomically Thin Nanosheets

By cutting the 3D bonding perovskites ABX<sub>3</sub> through (100) specific crystallographic direction, we can obtain the layered metal halide perovskites with a general formula (RNH<sub>2</sub>)<sub>A</sub><sub>m-1</sub>B<sub>m</sub>X<sub>3m+1</sub>, where R is a long chain organic amine, and m represents the number of octahedron layer. One extreme case is that m equals 1, where one single layer of inorganic metal halide frameworks is capped on both sides and isolated by organic layers, forming 2D layered perovskites. The optical and optoelectronic properties of 2D layer perovskites are fundamentally of great interest because of the electronic decoupling, e.g., strong quantum confinement,<sup>[26]</sup> dielectric screening,<sup>[27]</sup> and large exciton binding energy.<sup>[28]</sup>

The colloidal synthesis approach only produces ultrathin (few layers) 2D NSs with relatively small lateral size. In order to synthesize atomically thin 2D perovskites with large lateral size up to a few micrometers, a substrate-guided method involving solvent evaporation was developed.<sup>[29]</sup> A very dilute precursor solution was drop-casted onto a flat substrate (for example, SiO<sub>2</sub>/Si) and then dried under mild heating. A ternary dimethylformamide (DMF)–chlorobenzene (CB)–acetonitrile (AN) cosolvent was used here. CB acts as antisolvent and

reduces the solubility of perovskites in DMF, and AN is found to be important to grow high quality 2D NSs. Due to the limited solubility of precursors in AN and low boiling temperature of AN, ultrathin 2D perovskite sheets crystallize on the flat substrates as AN evaporates quickly. A better understanding of the growth mechanism still needs further study. The synthesized ultrathin (C<sub>4</sub>H<sub>9</sub>NH<sub>3</sub>)<sub>2</sub>PbBr<sub>4</sub> 2D sheets exhibit strong PL emission and a blue peak shift comparing to their bulk counterparts. The TEM characterizations show a lattice relaxation in PbBr<sub>4</sub><sup>2-</sup> layer in the 2D sheets (*a* = 8.45 Å, *b* = 8.67 Å) comparing to the bulk (*a* = 8.22 Å, *b* = 8.33 Å). Such structural change is attributed to the blue shift of the PL spectra of 2D sheets. The DFT simulation also suggests a 20 meV enlarged bandgap for the single-layer 2D sheets, which is a trend consistent with our experimental observations.

This growth method can also be generalized to other perovskite compositions. Different 2D sheets have been successfully synthesized as shown in Figure 2c, with compositions of (C<sub>4</sub>H<sub>9</sub>NH<sub>3</sub>)<sub>2</sub>PbCl<sub>4</sub> (i), (C<sub>4</sub>H<sub>9</sub>NH<sub>3</sub>)<sub>2</sub>PbI<sub>4</sub> (iii), (C<sub>4</sub>H<sub>9</sub>NH<sub>3</sub>)<sub>2</sub>PbCl<sub>2</sub>Br<sub>2</sub> (iv), (C<sub>4</sub>H<sub>9</sub>NH<sub>3</sub>)<sub>2</sub>PbBr<sub>2</sub>I<sub>2</sub> (v), and (C<sub>4</sub>H<sub>9</sub>NH<sub>3</sub>)<sub>2</sub>(CH<sub>3</sub>NH<sub>3</sub>)Pb<sub>2</sub>Br<sub>7</sub> (vi). These 2D sheets have well-defined shapes and wide wavelength tunability of emission. The excellent optical properties and solution processibility make the ultrathin 2D perovskites promising for further fundamental study in 2D materials and new nanoscale optoelectronic applications.

## 3. Anion Exchange and Heterojunctions

Ion-exchange reactions, which are partial or complete replacement of ions in a parent nanostructure by new guest ions, have been widely studied on II–VI, III–V, and IV–VI semiconductors.<sup>[30]</sup> Halide perovskites are known to exhibit the feature of high halide ion (X site) mobility and rigid cationic sublattice (B site), and therefore, facile anion-exchange reactions have been emerged as an effective way to achieve wide compositional and optical tunability in halide perovskites, and application in architecting perovskite heterostructures with distinguishing halide composition.

### 3.1. Anion Exchange Chemistry in Colloidal Nanowires

Fast anion-exchange reactions have been demonstrated in CsPbX<sub>3</sub> 0D NCs system.<sup>[31]</sup> However, the study of this strategy in CsPbX<sub>3</sub> 1D nanowire system was still lacking. Furthermore, anion-exchange strategy was expected to overcome the issues of low yield, poor diameter control and undesirable optical properties suffered from the direct synthesis of CsPbX<sub>3</sub> NWs (X = Cl, I).

CsPbBr<sub>3</sub> NWs with uniform diameters of 10 ± 2 nm were chosen as the starting material to achieve alloyed NWs with broad compositions by reacting with organic or inorganic halide precursors (such as oleylammonium halide and lead halide).<sup>[20]</sup> The anion-exchange reaction happens at the solid/liquid interface, which can be carried out in a toluene solvent with halide precursors in the presence of oleic acid and oleylamine at room temperature or a mild temperature (e.g., 80 °C) on an exchange time range from a few minutes to around 1 h. According to the

TEM and X-ray diffraction (XRD) characterizations, the original morphology (size and shape, **Figure 3a**) and crystal structure were maintained after anion-exchange process. The PL peaks of the CsPbBr<sub>3</sub> NWs blue shifted to shorter wavelengths when exchanged with Cl<sup>-</sup> precursor and finally reached the shortest wavelength at around 409 nm with increasing Cl ratio. Red shift to longer wavelength occurred when the CsPbBr<sub>3</sub> NWs were exchanged with I<sup>-</sup> precursor, and a value of 680 nm was eventually achieved by gradually increasing the I<sup>-</sup> content. The optical bandgap can be tuned from 1.8 to 2.9 eV by varying the percentage of different halides (**Figure 3b**) and a high PLQY was achieved after the anion-exchange reaction (Started Br, 53% ± 0.7%; exchanged I, 81% ± 2.5% and Cl, 30% ± 11%) (**Figure 3c**). This anion-exchange strategy can also be extended to the ultrathin NWs with diameter of 2.2 ± 0.2 nm without damage of the surface morphology and change of the crystal structure.<sup>[10b]</sup>

### 3.2. Halide Perovskite Heterojunction in Large Sized Nanowires

The anion-exchange reaction is facile and fast in colloidal perovskite NWs with small diameters. If the exchange reaction can be controlled locally at particular positions, then it is possible to create well-defined patterns of perovskite heterostructures with distinguishing halide species. The physical properties (optical, electrical, optoelectronic, etc.) of the heterostructures are

fundamentally interesting, and the spatially patterned semiconductor heterojunctions are essential for large-scale high-density optoelectronics, integration with well-established electronic systems and among others.

We have demonstrated spatial resolution anion exchange with individual CsPbBr<sub>3</sub> NW (with a few hundred nm width and micron scale length).<sup>[32]</sup> The NW is first coated with a layer of poly(methyl methacrylate) (PMMA). Then well-defined patterns of PMMA are removed via standard electron beam lithography techniques. The NW is then immersed in oleylammonium chloride/1-octadecene solution at room temperature, where only the exposed part performed the localized anion-exchange reaction. The mild reaction conditions are essential for preserving the nanowire morphology and creating high-quality heterojunctions. During the halide exchange from CsPbBr<sub>3</sub> to CsPbCl<sub>3</sub>, the PL peaks gradually shift from ≈525 to ≈420 nm, indicating the formation of halide alloy (CsPbBr<sub>3-x</sub>Cl<sub>x</sub>), instead of core-shell structures. After anion exchange, the PMMA layer can be completely removed by sequent washing in chlorobenzene and hexane. The resulting nanowire shows green-blue two colors PL emission with clear interface (**Figure 3d**). The two distinguishing PL peaks (≈420 and ≈525 nm) correspond to the emissions of CsPbCl<sub>3</sub> and CsPbBr<sub>3</sub>, respectively. Scanning electron microscopy (SEM) energy-dispersive X-ray spectroscopy mapping shows a sharp interface between the bromide and the chloride distributions along the nanowire, further confirming the formation

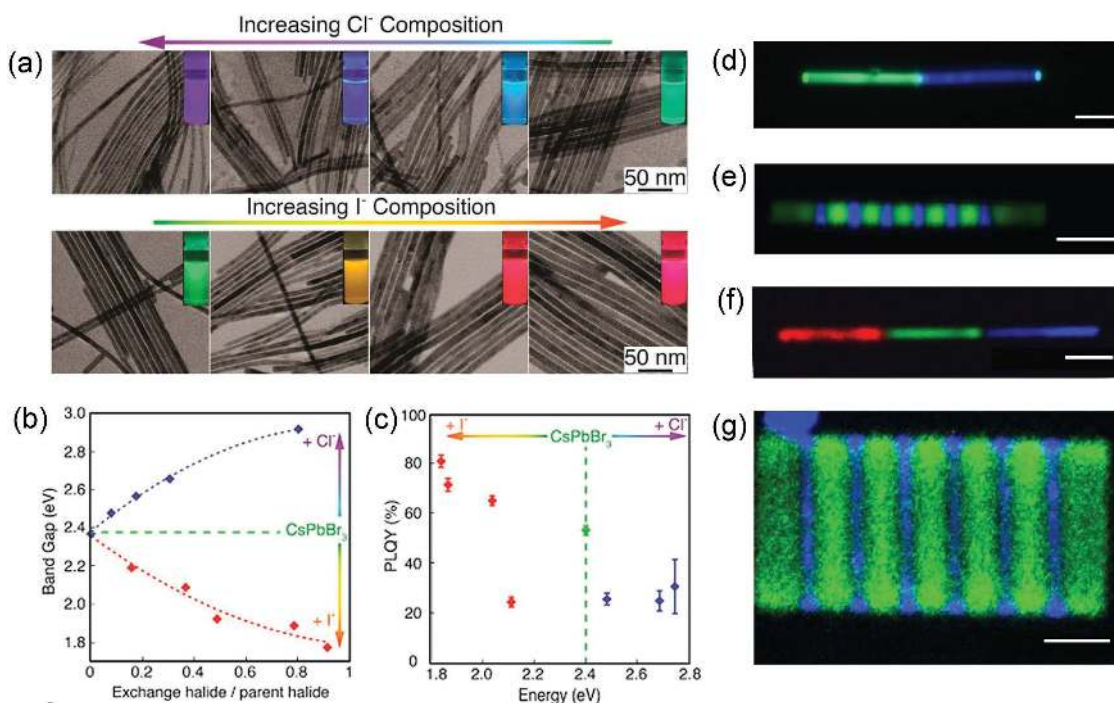


**Figure 3.** a) TEM images of CsPb(Br/Cl)<sub>3</sub> and CsPb(Br/I)<sub>3</sub> NWs with various degrees of conversion with chloride and iodide anions. The insets show the corresponding evolution of emission color (UV excitation,  $\lambda = 365$  nm). b) Plots of the absorption onset energy as a function of iodide or chloride percentage. c) Measured PLQY as a function of the bandgap energy of the exchanged NWs. a–c) Reproduced with permission.<sup>[20]</sup> Copyright 2016, ACS. d) PL images of CsPbBr<sub>3</sub>-CsPbCl<sub>3</sub> nanowire heterojunction under laser excitation. Confocal PL mapping of different types of heterojunctions including e) a CsPbBr<sub>3</sub>-CsPbCl<sub>3</sub> superlattice nanowire with pixel size of below 500 nm, f) a three-color of CsPbI<sub>3</sub> CsPbBr<sub>3</sub>-CsPbCl<sub>3</sub> heterojunction nanowire, and g) pattern on CsPbBr<sub>3</sub> plates. Blue color represents emission from 410 to 450 nm. Green color represents emission from 500 to 550 nm. Red color represents emission from 580 to 640 nm. All the scale bar is 3  $\mu$ m for (d) to (g). d–g) Reproduced with permission.<sup>[32]</sup> Copyright 2017, NAS.

of CsPbBr<sub>3</sub>–CsPbCl<sub>3</sub> heterojunction. The heterojunction has distinguishing electronic interface, which is systematically studied by scanning Kelvin probe force microscopy. The Br–I heterojunction can also be created when oleylammonium iodide/1-octadecene is used as the anion-exchange solution (Figure 3f). We demonstrate that the spatial resolution of the heterojunction can be down to 500 nm (Figure 3e,h). However, further attempt to 200 nm was not successful probably due to the spatial limitation of instruments or the interdiffusion of the anion species. These high-quality perovskite heterojunctions may represent as key building blocks for various optoelectronic applications, such as large-scale electronic circuit, high-density information storage, and high-resolution full color displays.

#### 4. Phase Transition Phenomena and Dynamics

Halide perovskite is a class of ionic material with a soft lattice compared to other photovoltaic semiconductor materials. This results in a highly reconfigurable crystal structure with relatively easy structural rearrangements induced by external stimuli to undergo a rich variety of solid–solid phase transitions. And during these structural phase transition processes, the physical properties (optical, electrical, electronic, magnetic, optoelectronic, etc.) of halide perovskite materials can be significantly altered, rendering promising potential applications in various optoelectronic devices, such as smart photovoltaics, photodetectors, and memory devices. However, the understanding of the phase transition phenomenon and mechanism, the structure evolution of the perovskites, and the connection between the structure and the properties is quite lacking.

Our recent research mainly focuses on the development of inorganic halide perovskites, which show rich structural phase transition behaviors and well control of the phase transitions via water and thermal heating. We introduce here the intrinsic phase transitions in individual CsPbI<sub>3</sub> NW, stabilization of perovskite phase through rapid thermal cooling procedures, and systematic study of the phase transition related optical and electrical properties.

Besides the fundamental study of the structural phase transition in NWs, we also demonstrate the design of a new class of thermochromic smart photovoltaic window device based on the structural phase transitions in cesium lead iodide/bromide (CsPbI<sub>3–x</sub>Br<sub>x</sub>). This provides a thread to broaden the further applications of phase transitions in inorganic halide perovskite materials.

##### 4.1. Phase Transition in CsPbI<sub>3</sub> and Optical and Electrical Properties

People have long been realized the inorganic perovskite shows the so-called “phase instability” phenomenon in humid air. In the pure iodide version, CsPbI<sub>3</sub> is stable in the perovskite phase (we call it black phase, or more generally, high-T phase) above 300–320 °C,<sup>[33]</sup> and quickly transits to the nonperovskite phase (yellow phase, or low-T phase) at room temperature,<sup>[34]</sup> which shows poor functionality, and with a corresponding color change from black to yellow. As a result, researchers have

focused on the stability enhancement of high-T phase when exposing to ambient conditions at room temperature, such as by chemical modification, doping, and ligand protections.<sup>[9,35]</sup>

In order to deeply understand the intrinsic phase transition properties in inorganic halide perovskite materials, we created a good platform-CsPbI<sub>3</sub> single-crystalline NWs synthesized by substrate-crystallization method introduced in Section 2.2.1. We find here that the as-prepared NWs is in their nonperovskite orthorhombic low-T phase, which is consisted of 1D double chains of edge-sharing PbI<sub>6</sub> octahedra, resulting in the preferable growth of 1D NWs. The transitions from the low-T to high-T phase can be realized by heating above 320 °C.<sup>[36]</sup> The inorganic halide perovskite remained in high-T phase by fast cooling. The postheated NWs show an orthorhombic phase with lower symmetry (compared to cubic phase) probably due to the lattice distortion. The high-T phase of CsPbI<sub>3</sub> obtained by heating above its phase transition temperature is actually a metastable phase at room temperature; by reheating at a lower temperature above 200 °C or exposure to moisture, it turns to the nonperovskite low-T phase again by rearranging the metal-halide octahedra (Figure 4a). As the phase transition processes are kinetically controlled, the phases of inorganic perovskite show bistability and can be changed back and forth reversibly.

The large structural rearrangement in CsPbI<sub>3</sub> NWs induced by phase transitions between the two phases is accompanied by complete changes in the optical and electronic properties between the two intrinsic characteristic states. For example, from the absorption spectra, the bandgap of high-T phase and low-T phase is about 1.76 and 2.78 eV, respectively. The PL intensity of high-T phase shows significant increase in relative intensity as compared with low-T phase (Figure 4b). From the PL image, we can find the low-T phase shows a low self-trapped blue emission, while the high-T phase shows the red band edge emission (Figure 4c,d). Furthermore, the photoconductivity of high-T phase is also much stronger than the low-T one, indicating the high-T phase is more photoactive and suitable for various applications.

The phenomenon of phase transitions in inorganic halide perovskites is significantly different from the intensively investigated hydration process in the organic–inorganic hybrid system;<sup>[37]</sup> or more generally, molecule intercalation that would cause the formation of new intermediate compounds,<sup>[38]</sup> although both of them can also alter the states and the optical properties of perovskite materials. The entire process of phase transition in inorganic perovskite system is highly stable, controllable, and fully reversible, which means intrinsic long-term thermal and environmental stability.

##### 4.2. Phase Transitions in Functional Photovoltaic Materials

As mentioned above, besides the great changes in absorption, PL intensity and photoconductivity, the color appearance is also changed significantly during phase transitions, one with high visible transparency and the other with very deep color which means strong light absorption with the ability to achieve high solar cell power output. This phenomenon was called thermochromic behavior.

Based on our understanding and extracted knowledge from phase transition, we first use rich structural phase transitions in



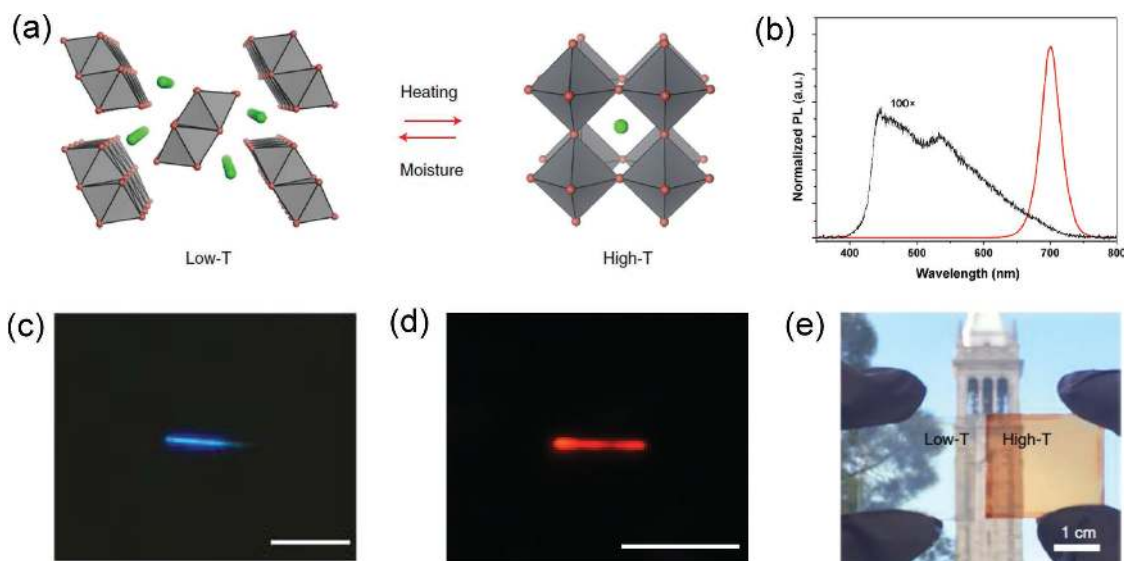


**Figure 4.** a) Schematics of phase transitions between low-T and high-T phases of inorganic halide perovskites with the general formula of  $\text{CsPbI}_{3-x}\text{Br}_x$ . Reproduced with permission.<sup>[39]</sup> Copyright 2018, Springer Nature. b) Normalized PL spectra of low-T phase (black line) and high-T phase (red line)  $\text{CsPbI}_3$  NWs. Reproduced with permission.<sup>[36]</sup> Copyright 2016, Springer Nature. c, d) PL images of low-T (c) and high-T (d) phase  $\text{CsPbI}_3$  NWs. Reproduced with permission.<sup>[36]</sup> Copyright 2016, Springer Nature. The scale bar is 10  $\mu\text{m}$ . e) A demonstration of smart photovoltaic windows using the phase transition behaviors. Reproduced with permission.<sup>[39]</sup> Copyright 2018, Springer Nature.

alloyed inorganic halide perovskite materials to realize switchable smart photovoltaic (PV) windows, showing both photoactivity (high-T phase) and chromic features (low-T phase, Figure 4e).<sup>[39]</sup> In comparison to existing non-PV chromic windows,<sup>[40]</sup> additional electricity can be produced in modern smart buildings.

To achieve this, we exploit the controlling of phase transitions in inorganic  $\text{CsPbI}_{3-x}\text{Br}_x$  perovskites between the low-T phase (transparent state) and the high-T phase (dark light-absorbing state). For  $\text{CsPbI}_3$ , the high-T phase can be transitioned to the low-T phase by reheating. When Br is added, the high-T phase of  $\text{CsPbI}_{3-x}\text{Br}_x$  is more stable without full reversibility by just heating, indicating that the energy barrier across the transition would be higher compared with the pure iodide one. We find that the moisture treatment is a general approach to realize the full reversibility. The phase transition rate shows the strong dependence on relative humidity as well as the composition (Br/I ratio).

The underlying mechanism of the moisture-triggered phase transitions in this type of inorganic perovskite is disclosed in detail both experimentally and theoretically in our work. The quantified results evidence that water has only a catalytic effect, which can trigger the phase transition by creating vacancies and reducing the solid–solid surface tension between the two phases. We also developed other catalysts, such as methanol and ethanol, to trigger the phase transitions. The results show that the “moisture triggered phase transition” is a surface phenomenon.

Based on the phenomenon and mechanistic studies of phase transitions in this alloyed perovskites, we utilize them as smart PV window active materials. By incorporating suitable interlayers and contact materials, this system can be reversibly switched between an absorbing configuration in which it produces electricity and a nonabsorbing configuration which acts as a window.

The so-called thermochromic solar cells has the advantages of great tunability in composition, thus we can design inorganic halide perovskites with tunable properties that include absorption, color, transition temperatures and procedures, phase stability, PV performance, and transmittance modulation range. As the first generation of smart PV windows, we chose the composition  $\text{CsPbIBr}_2$  in order to achieve the moderate phase stability, low transition temperature, and to reach a balance between the power output and the window color/transparency. It has the huge probability to optimize the perovskite materials toward practical applications.

## 5. Photonics and Thermoelectric Applications

Controlling and manipulating photons in nanoscale semiconductor crystals can lead to advancing the field of photonics,<sup>[16]</sup> including commercial applications in communications,<sup>[41]</sup> sensing,<sup>[42]</sup> imaging,<sup>[43]</sup> and data storage.<sup>[44]</sup> Nanowire lasers show the promising features as such miniaturized photonics. Semiconductor NWs may be easily integrated into optoelectronic circuits because of their small size and their potential in electrical pumping.<sup>[14,45]</sup> People have realized nanowire lasers in a variety of II–VI and III–V semiconductors.<sup>[46]</sup> Yet these NWs require high cost and high power consumption synthetic conditions, and have limited emission wavelength tunability. Discovery or searching of new class of semiconductor NWs with low cost and wide wavelength tunability is still challenging.

Phonon transport is expected to be greatly hampered in thin semiconductor 1D NWs because of increased boundary scattering and reduced phonon group velocities. As a result, the low thermal conductivity of nanowires is advantageous for thermoelectric applications, which are characterized by the figure-of-merit ( $ZT = \sigma S^2 T / (\kappa_1 + \kappa_2)$ ), with  $\sigma$ ,  $S$ ,  $T$ ,  $\kappa_1$ , and  $\kappa_2$ : electronic conductivity, the Seebeck coefficient, absolute

temperature, lattice thermal conductivity, and electronic thermal conductivity, respectively. Therefore, semiconductor nanowires with desired and tunable size, composition and carrier concentration are promising candidates for boosting the thermoelectric performances.

### 5.1. Optically Driven Lasers

Recently halide perovskites have been found to own low trap state density and high PLQY.<sup>[47]</sup> These excellent optoelectronics, together with solution-phase processability and wide tunability, make them attractive as next generation photonic applications.<sup>[2a,8]</sup> As good optical gain medium, either polycrystalline thin film or colloidal quantum dots show amplified spontaneous emission (ASE) at low excitation threshold.<sup>[4a,48]</sup> Acting as the laser cavity and gain medium, inorganic perovskite NWs are promising candidates for robust and efficient nanoscale lasers. The colloidal CsPbX<sub>3</sub> NWs are too narrow (<20 nm diameter) to efficiently support photonic lasing modes. As we discussed in Section 2.2.1, we utilize the substrate-guided method here to grow single-crystal CsPbX<sub>3</sub> NWs (with a few hundred nm in width and micron scale in length). These NWs have well-defined facets and ideal size region for nanowire lasing. When the optical pumping surpasses the threshold, stimulated emission dominates and a lasing emission pattern is observed with CsPbBr<sub>3</sub> NW, showing the interference of the coherent emission from the two end facets of the nanowire (Figure 5a). Fabry-Pérot lasing modes were observed in CsPbBr<sub>3</sub> NWs with a low threshold of 5 μJ cm<sup>-2</sup> (Figure 5b).<sup>[24a]</sup> CsPbX<sub>3</sub> perovskites were shown to be stable to heat or moisture comparing to organic-inorganic counterparts.<sup>[49]</sup> The CsPbX<sub>3</sub> nanowire exhibits stable lasing over 10<sup>9</sup> excitation cycles and persists even exposed to ambient atmosphere. Integrating nanostructures with electronic systems is the next challenge to advanced photonic device applications.

### 5.2. Thermoelectric Application

The transport properties of nanomaterials can be prior to their bulk counterparts.<sup>[50]</sup> Semiconductor NWs represent lower thermal conductivity if their diameter is smaller than phonon mean free path length. Discovery of novel materials with extreme thermal transport properties is another approach for manipulation and utilization of thermal energy.<sup>[18]</sup> Single crystals with ultralow thermal conductivity are particularly of great interest, which are desired for turbine engines,<sup>[51]</sup> thermal data storage devices,<sup>[44]</sup> and thermoelectric devices.<sup>[52]</sup> Very few studies have been performed for thermal conductivity of halide perovskites. An ultralow thermal conductivity of 0.5 W m<sup>-1</sup> K<sup>-1</sup> has been reported for bulk CH<sub>3</sub>NH<sub>3</sub>PbI<sub>3</sub>.<sup>[53]</sup> Computational study shows that the main contribution for the ultralow thermal conductivity is rotational motions of organic CH<sub>3</sub>NH<sub>3</sub><sup>+</sup> ion.<sup>[54]</sup> Due to the limited investigations of thermal transport in halide perovskites, fundamental understanding of thermal transport still remains highly elusive.

In order to characterize the transport properties, individual perovskite NW (CsPbI<sub>3</sub>, CsPbBr<sub>3</sub> or CsSnI<sub>3</sub>) is suspended

between two membranes (Figure 5c). The thermal conductivity, electrical conductivity, and Seebeck coefficient can be measured on individual single NW. We observe remarkably ultralow thermal conductivity in these perovskite nanowires (CsPbI<sub>3</sub>, 0.45 ± 0.05 W m<sup>-1</sup> K<sup>-1</sup>, CsPbBr<sub>3</sub>, 0.42 ± 0.04 W m<sup>-1</sup> K<sup>-1</sup>, and CsSnI<sub>3</sub>, 0.38 ± 0.04 W m<sup>-1</sup> K<sup>-1</sup>, Figure 5d).<sup>[25]</sup> The values are comparable to and even smaller than various crystals with well-known low lattice thermal conductivity.<sup>[51]</sup> Besides, the ratio of lattice thermal conductivity to estimated minimum values at room temperature is only ≈2 for all NWs (Figure 5d, inset). This ratio is smaller than that of other crystals with low thermal conductivity. Ultralow thermal conductivity is attributed to the cluster rattling effect, where strong optical-acoustic phonon scatterings are induced in halide perovskite lattice. Extremely short maximum mean-free path is attributed by dramatic anharmonicity due to such cluster rattling mechanism. Replacing Pb with Sn in the B site, electrical properties change tremendously to high electrical conductivity (282 S cm<sup>-1</sup>), and high hole mobility (394 cm<sup>2</sup> V<sup>-1</sup> s<sup>-1</sup>). By precisely controlling the alloy ratio in CsPb<sub>x</sub>Sn<sub>1-x</sub>X<sub>3</sub>, the transport properties can be widely tuned. These alloy perovskites are promising for further applications in photonic and thermoelectric devices.

## 6. Future Work and Challenges

In this report, we have summarized our recent progress and contribution made to the inorganic halide perovskites field over the past three years. Future directions and challenges we are going to pursuit are mainly as follows:

Inorganic halide perovskites have the advantage in the stability toward moisture, light, and heat, and there are growing efforts in improving their optical properties for further applications. Surface treatment, in terms of tuning the stoichiometric ratio and doing the surface passivation, is one of the feasible ways to address this issue. New compositions tuning such as mixing of A, B, X sites, and structures design such as double perovskites and layered perovskites, are also promising.

Anion-exchange reactions have been carried out on halide perovskites in terms of 0D, 1D, and 2D colloidal nanocrystals as well as individual NWs/NPLs to make the well-defined colorful patterns. However, the anion-exchange kinetics on time and spatial scale are still elusive. More insight understanding can enable the precise control of compositions and structures. Furthermore, comparing to the anion exchange, cation exchange is sluggish due to the rigid cationic sublattice. Only partial cation exchange has been demonstrated, and new strategies and dynamics need to be investigated.

The toxicity of lead is a main concern for the large-scale utilization of lead halide perovskites in various applications such as photovoltaics and color-tunable light emitting diodes. The development of environmentally benign lead-free halide perovskites with comparable excellent features and exploration of their fundamental optical and electronic properties and environmental stability are interesting, such as Cs<sub>2</sub>AgBiX<sub>6</sub>, Cs<sub>3</sub>Bi<sub>2</sub>X<sub>9</sub>, Cs<sub>3</sub>Sb<sub>2</sub>X<sub>9</sub>, and others analogues.<sup>[55]</sup>

In summary, many progresses have been achieved in inorganic halide perovskites including synthesis, structure

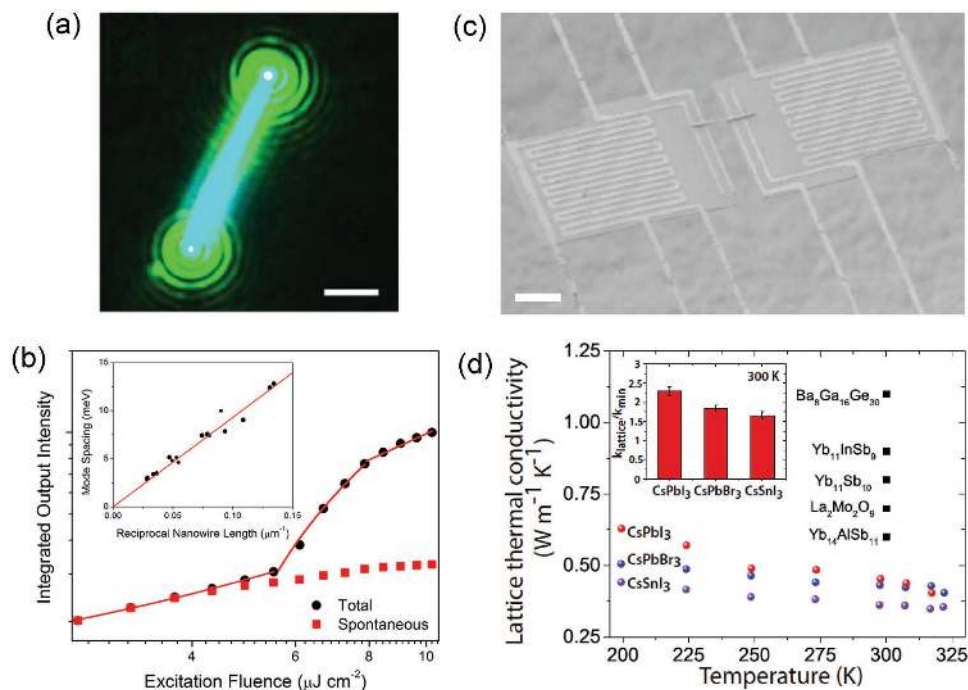


**Figure 5.** a) Lasing in single-crystalline CsPbBr<sub>3</sub> NW. Scale bar: 2 μm. b) The integrated output intensity of the CsPbBr<sub>3</sub> NW with increasing pump fluence (black circles) follows a typical S-curve pattern. Spontaneous emission (red squares) from the NW plateaus as stimulated emission begins to dominate after excitation fluence surpasses the threshold. The inset is plot of inverse nanowire length against mode spacing, confirming that Fabry–Pérot-type lasing is dominant. Reproduced with permission.<sup>[24a]</sup> Copyright 2016, NAS. c) SEM image of the suspended microisland device. Individual inorganic halide perovskites NW is suspended between two membranes. Scale bar: 10 μm. d) Lattice thermal conductivity of inorganic perovskites and other single crystals. (Inset) Ratio of lattice thermal conductivity to the minimum thermal conductivity for inorganic halide perovskites NWs. Reproduced with permission.<sup>[25]</sup> Copyright 2017, NAS.

characterization and applications. Much more progress toward new materials development, improvement of optical properties, and deeper fundamental understanding of composition–structure–property relationship and better performance of the devices need to be promoted in the near future.

## Acknowledgements

This work was supported by the U.S. Department of Energy, Office of Science, Office of Basic Energy Sciences, Materials Sciences and Engineering Division, under Contract DE-AC02-05-CH11231 within the Physical Chemistry of Inorganic Nanostructures Program (KC3103). M.L. acknowledges the fellowship support from Suzhou Industrial Park. J.L. acknowledges the fellowship support from Shanghai University of Electric Power.

## Conflict of Interest

The authors declare no conflict of interest.

## Keywords

anion exchange, nanowires, optoelectronic, phase transition, thermoelectrics

Received: May 3, 2018  
Revised: June 29, 2018  
Published online: September 10, 2018

- [1] a) M. A. Green, A. Ho-Baillie, H. J. Snaith, *Nat. Photonics* **2014**, *8*, 506; b) J. S. Manser, J. A. Christians, P. V. Kamat, *Chem. Rev.* **2016**, *116*, 12956; c) S. D. Stranks, H. J. Snaith, *Nat. Nanotechnol.* **2015**, *10*, 391.
- [2] a) M. M. Lee, J. Teuscher, T. Miyasaka, T. N. Murakami, H. J. Snaith, *Science* **2012**, *338*, 643; b) J. Burschka, N. Pellet, S.-J. Moon, R. Humphry-Baker, P. Gao, M. K. Nazeeruddin, M. Grätzel, *Nature* **2013**, *499*, 316; c) H. Zhou, Q. Chen, G. Li, S. Luo, T.-b. Song, H.-S. Duan, Z. Hong, J. You, Y. Liu, Y. Yang, *Science* **2014**, *345*, 542; d) N. J. Jeon, J. H. Noh, W. S. Yang, Y. C. Kim, S. Ryu, J. Seo, S. I. Seok, *Nature* **2015**, *517*, 476.
- [3] Z.-K. Tan, R. S. Moggaddam, M. L. Lai, P. Docampo, R. Higler, F. Deschler, M. Price, A. Sadhanala, L. M. Pazos, D. Credgington, F. Hanusch, T. Bein, H. J. Snaith, R. H. Friend, *Nat. Nanotechnol.* **2014**, *9*, 687.
- [4] a) G. Xing, N. Mathews, S. S. Lim, N. Yantara, X. Liu, D. Sabba, M. Grätzel, S. Mhaisalkar, T. C. Sum, *Nat. Mater.* **2014**, *13*, 476; b) Q. Zhang, S. T. Ha, X. Liu, T. C. Sum, Q. Xiong, *Nano Lett.* **2014**, *14*, 5995; c) H. Zhu, Y. Fu, F. Meng, X. Wu, Z. Gong, Q. Ding, M. V. Gustafsson, M. T. Trinh, S. Jin, X. Y. Zhu, *Nat. Mater.* **2015**, *14*, 636.
- [5] NREL best research-cell efficiencies: efficiency chart, <https://www.nrel.gov/pv/assets/images/efficiency-chart.png> (accessed: August 2018).
- [6] W. S. Yang, B.-W. Park, E. H. Jung, N. J. Jeon, Y. C. Kim, D. U. Lee, S. S. Shin, J. Seo, E. K. Kim, J. H. Noh, S. I. Seok, *Science* **2017**, *356*, 1376.
- [7] a) J. W. Lee, D. H. Kim, H. S. Kim, S. W. Seo, M. Cho Sung, N. G. Park, *Adv. Energy Mater.* **2015**, *5*, 1501310; b) M. Saliba, T. Matsui, J.-Y. Seo, K. Domanski, J.-P. Correa-Baena, M. K. Nazeeruddin, S. M. Zakeeruddin, W. Tress, A. Abate, A. Hagfeldt, M. Grätzel, *Energy Environ. Sci.* **2016**, *9*, 1989; c) D. P. McMeekin, G. Sadoughi, W. Rehman, G. E. Eperon, M. Saliba,

- M. T. Hö rantner, A. Haghighirad, N. Sakai, L. Korte, B. Rech, M. B. Johnston, L. M. Herz, H. J. Snaith, *Science* **2016**, 351, 151.
- [8] S.-T. Ha, R. Su, J. Xing, Q. Zhang, Q. Xiong, *Chem. Sci.* **2017**, 8, 2522.
- [9] L. Protesescu, S. Yakunin, M. I. Bodnarchuk, F. Krieg, R. Caputo, C. H. Hendon, R. X. Yang, A. Walsh, M. V. Kovalenko, *Nano Lett.* **2015**, 15, 3692.
- [10] a) D. Zhang, S. W. Eaton, Y. Yu, L. Dou, P. Yang, *J. Am. Chem. Soc.* **2015**, 137, 9230; b) D. Zhang, Y. Yu, Y. Bekenstein, A. B. Wong, A. P. Alivisatos, P. Yang, *J. Am. Chem. Soc.* **2016**, 138, 13155; c) M. Imran, F. Di Stasio, Z. Dang, C. Canale, A. H. Khan, J. Shamsi, R. Brescia, M. Prato, L. Manna, *Chem. Mater.* **2016**, 28, 6450; d) J. Chen, Y. Fu, L. Samad, L. Dang, Y. Zhao, S. Shen, L. Guo, S. Jin, *Nano Lett.* **2017**, 17, 460.
- [11] a) Y. Bekenstein, B. A. Koscher, S. W. Eaton, P. Yang, A. P. Alivisatos, *J. Am. Chem. Soc.* **2015**, 137, 16008; b) J. Shamsi, Z. Dang, P. Bianchini, C. Canale, F. Di Stasio, R. Brescia, M. Prato, L. Manna, *J. Am. Chem. Soc.* **2016**, 138, 7240; c) J. Chen, D. J. Morrow, Y. Fu, W. Zheng, Y. Zhao, L. Dang, M. J. Stolt, D. D. Kohler, X. Wang, K. J. Czech, M. P. Hautzinger, S. Shen, L. Guo, A. Pan, J. C. Wright, S. Jin, *J. Am. Chem. Soc.* **2017**, 139, 13525.
- [12] a) M. C. Brennan, J. E. Herr, T. S. Nguyen-Beck, J. Zinna, S. Draguta, S. Rouvimov, J. Parkhill, M. Kuno, *J. Am. Chem. Soc.* **2017**, 139, 12201; b) <http://nptel.ac.in/courses/115106076/Module7/Module7.pdf> (accessed: June 2018).
- [13] A. P. Alivisatos, *Science* **1996**, 271, 933.
- [14] M. H. Huang, S. Mao, H. Feick, H. Yan, Y. Wu, H. Kind, E. Weber, R. Russo, P. Yang, *Science* **2001**, 292, 1897.
- [15] Q. H. Wang, K. Kalantar-Zadeh, A. Kis, J. N. Coleman, M. S. Strano, *Nat. Nanotechnol.* **2012**, 7, 699.
- [16] R. Yan, D. Gargas, P. Yang, *Nat. Photonics* **2009**, 3, 569.
- [17] B. Tian, T. J. Kempa, C. M. Lieber, *Chem. Soc. Rev.* **2009**, 38, 16.
- [18] A. I. Hochbaum, R. Chen, R. D. Delgado, W. Liang, E. C. Garnett, M. Najarian, A. Majumdar, P. Yang, *Nature* **2008**, 451, 163.
- [19] F. Patolsky, C. M. Lieber, *Mater. Today* **2005**, 8, 20.
- [20] D. Zhang, Y. Yang, Y. Bekenstein, Y. Yu, N. A. Gibson, A. B. Wong, S. W. Eaton, N. Kornienko, Q. Kong, M. Lai, A. P. Alivisatos, S. R. Leone, P. Yang, *J. Am. Chem. Soc.* **2016**, 138, 7236.
- [21] L. Cademartiri, G. A. Ozin, *Adv. Mater.* **2009**, 21, 1013.
- [22] a) D. D. D. Ma, C. S. Lee, F. C. K. Au, S. Y. Tong, S. T. Lee, *Science* **2003**, 299, 1874; b) D. Katz, T. Wizansky, O. Millo, E. Rothenberg, T. Mokari, U. Banin, *Phys. Rev. Lett.* **2002**, 89, 086801.
- [23] Y. Yu, D. Zhang, C. Kisielowski, L. Dou, N. Kornienko, Y. Bekenstein, A. B. Wong, A. P. Alivisatos, P. Yang, *Nano Lett.* **2016**, 16, 7530.
- [24] a) S. W. Eaton, M. Lai, N. A. Gibson, A. B. Wong, L. Dou, J. Ma, L.-W. Wang, S. R. Leone, P. Yang, *Proc. Natl. Acad. Sci. USA* **2016**, 113, 1993; b) A. B. Wong, M. Lai, S. W. Eaton, Y. Yu, E. Lin, L. Dou, A. Fu, P. Yang, *Nano Lett.* **2015**, 15, 5519.
- [25] W. Lee, H. Li, A. B. Wong, D. Zhang, M. Lai, Y. Yu, Q. Kong, E. Lin, J. J. Urban, J. C. Grossman, P. Yang, *Proc. Natl. Acad. Sci. USA* **2017**, 114, 8693.
- [26] R. Tamaki, Y. Arai, D. Ichikawa, M. Inoue, H. Kunugita, K. Ema, *J. Lumin.* **2008**, 128, 842.
- [27] T. Ishihara, *J. Lumin.* **1994**, 60, 269.
- [28] Y. Kato, D. Ichii, K. Ohashi, H. Kunugita, K. Ema, K. Tanaka, T. Takahashi, T. Kondo, *Solid State Commun.* **2003**, 128, 15.
- [29] L. Dou, A. B. Wong, Y. Yu, M. Lai, N. Kornienko, S. W. Eaton, A. Fu, C. G. Bischak, J. Ma, T. Ding, *Science* **2015**, 349, 1518.
- [30] S. Gupta, S. V. Kershaw, A. L. Rogach, *Adv. Mater.* **2013**, 25, 6923.
- [31] Q. A. Akkerman, V. D'Innocenzo, S. Accornero, A. Scarpellini, A. Petrozza, M. Prato, L. Manna, *J. Am. Chem. Soc.* **2015**, 137, 10276.
- [32] L. Dou, M. Lai, C. S. Kley, Y. Yang, C. G. Bischak, D. Zhang, S. W. Eaton, N. S. Ginsberg, P. Yang, *Proc. Natl. Acad. Sci. USA* **2017**, 114, 7216.
- [33] a) C. K. Möller, *Nature* **1958**, 182, 1436; b) M. Natarajan, B. Prakash, *Phys. Status Solidi A* **1971**, 4, K167.
- [34] G. E. Eperon, G. M. Paternò, R. J. Sutton, A. Zampetti, A. A. Haghighirad, F. Cacialli, H. J. Snaith, *J. Mater. Chem. A* **2015**, 3, 19688.
- [35] a) A. Swarnkar, A. R. Marshall, E. M. Sanehira, B. D. Chernomordik, D. T. Moore, J. A. Christians, T. Chakrabarti, J. M. Luther, *Science* **2016**, 354, 92; b) P. Luo, W. Xia, S. Zhou, L. Sun, J. Cheng, C. Xu, Y. Lu, *J. Phys. Chem. Lett.* **2016**, 7, 3603; c) S. Dastidar, D. A. Egger, L. Z. Tan, S. B. Cromer, A. D. Dillon, S. Liu, L. Kronik, A. M. Rappe, A. T. Fafarman, *Nano Lett.* **2016**, 16, 3563.
- [36] M. Lai, Q. Kong, C. G. Bischak, Y. Yu, L. Dou, S. W. Eaton, N. S. Ginsberg, P. Yang, *Nano Res.* **2017**, 10, 1107.
- [37] a) J. A. Christians, P. A. Miranda Herrera, P. V. Kamat, *J. Am. Chem. Soc.* **2015**, 137, 1530; b) A. I. M. Leguy, Y. Hu, M. Campoy-Quiles, M. I. Alonso, O. J. Weber, P. Azarhoosh, M. Van Schilfgaarde, M. T. Weller, T. Bein, J. Nelson, *Chem. Mater.* **2015**, 27, 3397; c) A. Halder, D. Choudhury, S. Ghosh, A. S. Subbiah, S. K. Sarkar, *J. Phys. Chem. Lett.* **2015**, 6, 3180.
- [38] a) X. Guo, C. McCleese, C. Kolodziej, A. C. Samia, Y. Zhao, C. Burda, *Dalton Trans.* **2016**, 45, 3806; b) L. M. Wheeler, D. T. Moore, R. Ihly, N. J. Stanton, E. M. Miller, R. C. Tenent, J. L. Blackburn, N. R. Neale, *Nat. Commun.* **2017**, 8, 1722.
- [39] J. Lin, M. Lai, L. Dou, C. S. Kley, H. Chen, F. Peng, J. Sun, D. Lu, S. A. Hawks, C. Xie, F. Cui, A. P. Alivisatos, D. T. Limmer, P. Yang, *Nat. Mater.* **2018**, 17, 261.
- [40] a) G. A. Niklasson, C. G. Granqvist, *J. Mater. Chem.* **2007**, 17, 127; b) C. G. Granqvist, *Sol. Energy Mater. Sol. Cells* **2000**, 60, 201.
- [41] R. G. Beausoleil, P. J. Kuekes, G. S. Snider, S.-Y. Wang, R. S. Williams, *IEEE* **2008**, 96, 230.
- [42] R. Yan, J.-H. Park, Y. Choi, C.-J. Heo, S.-M. Yang, L. P. Lee, P. Yang, *Nat. Nanotechnol.* **2012**, 7, 191.
- [43] Y. Nakayama, P. J. Pauzauskie, A. Radenovic, R. M. Onorato, R. J. Saykally, J. Liphardt, P. Yang, *Nature* **2007**, 447, 1098.
- [44] L. Pan, D. B. Bogy, *Nat. Photonics* **2009**, 3, 189.
- [45] X. Duan, Y. Huang, R. Agarwal, C. M. Lieber, *Nature* **2003**, 421, 241.
- [46] a) W. Shi, Y. F. Zheng, N. Wang, C.-S. Lee, S.-T. Lee, *Adv. Mater.* **2001**, 13, 591; b) J. C. Johnson, H.-J. Choi, K. P. Knutsen, R. D. Schaller, P. Yang, R. J. Saykally, *Nat. Mater.* **2002**, 1, 106.
- [47] a) D. Shi, V. Adinolfi, R. Comin, M. Yuan, E. Alarousu, A. Buin, Y. Chen, S. Hoogland, A. Rothenberger, K. Katsiev, Y. Losovyj, X. Zhang, P. A. Dowben, O. F. Mohammed, E. H. Sargent, O. M. Bakr, *Science* **2015**, 347, 519; b) B. A. Koscher, J. K. Swabeck, N. D. Bronstein, A. P. Alivisatos, *J. Am. Chem. Soc.* **2017**, 139, 6566.
- [48] S. Yakunin, L. Protesescu, F. Krieg, M. I. Bodnarchuk, G. Nedelcu, M. Humer, G. De Luca, M. Fiebig, W. Heiss, M. V. Kovalenko, *Nat. Commun.* **2015**, 6, 8056.
- [49] G. Niu, X. Guo, L. Wang, *J. Mater. Chem. A* **2015**, 3, 8970.
- [50] D. Li, Y. Wu, P. Kim, L. Shi, P. Yang, A. Majumdar, *App. Phys. Lett.* **2003**, 83, 2934.
- [51] E. S. Toberer, A. Zevalkink, G. J. Snyder, *J. Mater. Chem.* **2011**, 21, 15843.
- [52] G. J. Snyder, E. S. Toberer, *Nat. Mater.* **2008**, 7, 105.
- [53] A. Pisoni, J. Jacimovic, O. S. Barisic, M. Spina, R. Gaál, L. Forró, E. Horváth, *J. Phys. Chem. Lett.* **2014**, 5, 2488.
- [54] S.-Y. Yue, X. Zhang, G. Qin, J. Yang, M. Hu, *Phys. Rev. B* **2016**, 94, 115427.
- [55] a) A. B. Wong, Y. Bekenstein, J. Kang, C. S. Kley, D. Kim, N. A. Gibson, D. Zhang, Y. Yu, S. R. Leone, L.-W. Wang, A. P. Alivisatos, P. Yang, *Nano Lett.* **2018**, 18, 2060; b) A. H. Slavney, T. Hu, A. M. Lindenberger, H. I. Karunadasa, *J. Am. Chem. Soc.* **2016**, 138, 2138; c) B. Yang, J. Chen, F. Hong, X. Mao, K. Zheng, S. Yang, Y. Li, T. Pullerits, W. Deng, K. Han, *Angew. Chem., Int. Ed.* **2017**, 56, 12471.